Phys. Status Solidi B **252,** No. 5, 1031–1037 (2015) / **DOI** 10.1002/pssb.201451590

physica status solidi b
www.pss-b.com
basic solid state physics

Electrical characteristics of low-Mg-doped p-AlGaN and p-InGaN Schottky contacts

Toshichika Aoki*, Sachi Tachibana, and Kenji Shiojima

Graduate School of Electrical and Electronics Engineering, University of Fukui, 3-9-1 Bunkyo, Fukui 910-8507, Japan

Received 30 September 2014, revised 24 January 2015, accepted 26 January 2015
Published online 18 February 2015

Keywords AlGaN, doping, electrical properties, InGaN, magnesium, Schottky contacts

* Corresponding author: e-mail aoki0529@u-fukui.ac.jp, Phone: +81-776-27-8560, Fax: +81-776-27-8749

Electrical characteristics of low-Mg-doped p-$Al_{0.02–0.07}Ga_{0.98–0.93}N$ and p-$In_{0.02}Ga_{0.98}N$ Schottky contacts were investigated. A memory effect was revealed in the current–voltage (I–V) characteristics, which is found also in p-GaN contacts and may be due to charge and discharge of holes to acceptor-type interfacial defects. High-temperature isothermal transient spectroscopy revealed that the defect densities in the $Al_{0.02}Ga_{0.98}N$ and $In_{0.02}Ga_{0.98}N$ samples were nearly half that in the GaN samples. A large reverse current with a memory effect was observed in the $In_{0.02}Ga_{0.98}N$ contacts. It was suggested that current can flow via relatively shallow acceptor-type interfacial defects. For the $Al_xGa_{1-x}N$ with $x = 0.04$ and 0.07, I–V characteristics became leaky. The Schottky barrier heights estimated from the photoresponse experiment were higher than the values estimated from the bandgap by 0.19, 0.21, 0.20, and 0.21 eV for $Al_{0.02}Ga_{0.98}N$, $Al_{0.04}Ga_{0.96}N$, $Al_{0.07}Ga_{0.93}N$, and $In_{0.02}Ga_{0.98}N$ samples, respectively. A probable explanation for such discrepancies may be due to the total charge amount of the interfacial states, which varied the electric field and the barrier lowering. It was found that even though the Al or In content was only as small as 2%, the electrical characteristics of the contacts changed significantly.

1 Introduction Blue light-emitting diodes based on nitride semiconductors have become of major commercial significance since the first device was demonstrated [1]. In particular, blue light-emitting diodes and violet laser diodes serve in numerous applications including lighting and those in next-generation optical storage systems. While $Al_xGa_{1-x}N$ alloys are important for deep ultraviolet emitters, $In_xGa_{1-x}N$ alloys with bandgaps ranging from 0.7 to 3.4 eV cover the entire visible spectrum, thereby inspiring many future optoelectronics applications especially for green laser diodes. For the light emitting devices, the most important technology is epitaxial growth of active layers, however, it is known to be difficult to form a good ohmic contact. In comparison with n-type GaN, it is very difficult to form good ohmic contacts on p-type GaN. Many research groups have studied ohmic contacts to p-GaN with regard to electrode metals, annealing condition, and surface treatment around 1999 [2–5]. The ohmic contact formation thus has yet been established. As a practical way, a Au/Ni contact was formed on a heavily doped p-GaN, and subsequently annealed. There we find some reports on metal/n-AlGaN and n-InGaN contacts [6–8]. However, we found none for the p-type contacts.

We have studied Schottky electrodes to reinforce the basic understanding of p-GaN electrodes. We have reported for Ni/low-Mg-doped c-plane p-GaN a Schottky barrier height ($q\phi_B$) as high as 2.4 eV, a strong Fermi-level pinning, and a memory effect due to charge and discharge of acceptor-type defects in the vicinity of the interface [9–11]. We have expanded this study to Ni/p-AlGaN and Ni/p-InGaN contacts with relatively high Al or In contents up to 16% and Mg-doping concentration of $2 \times 10^{19}\,cm^{-3}$. In the current–voltage (I–V) characteristics, $q\phi_B$ could not be obtained due to large leakage currents, as shown in Fig. 1. In order to suppress the leakage current, we reconsidered the sample structure and lowered the Al or In composition and also the Mg-doping concentration.

In this study, we report the electrical characteristics of low-Mg-doped p-AlGaN and p-InGaN contacts with Al contents of 2–7% and an In content of as low as 2%. We have studied the current-transport mechanism by I–V and photoresponse (PR) measurements and we studied the

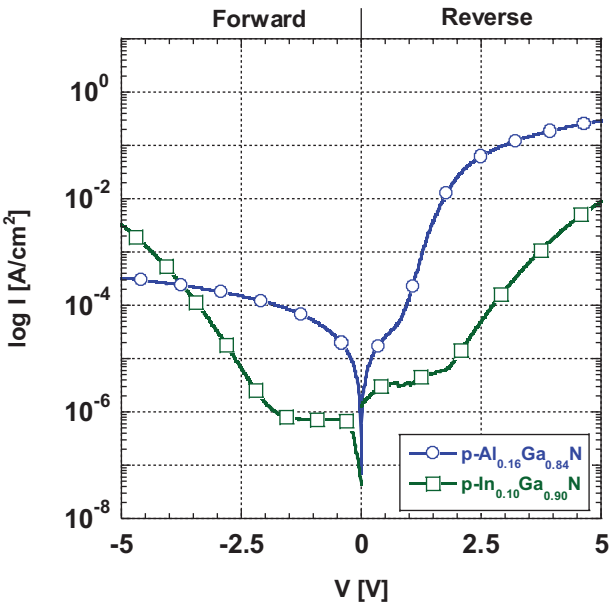

Figure 1 Typical I–V curves of p-$Al_{0.16}Ga_{0.84}N$ and p-$In_{0.10}Ga_{0.90}N$ contacts with Mg-doping concentration of $2 \times 10^{19}\,cm^{-3}$.

interfacial defects by high-temperature isothermal capacitance transient spectroscopy (H-ICTS).

2 Sample preparation and measurement conditions We fabricated lateral Schottky diodes shown in Fig. 2. Free-standing c-plane n-GaN (0001) substrates were used to obtain a better crystal quality by metalorganic chemical vapor deposition (MOCVD). The dislocation density was as low as $1 \times 10^6\,cm^{-2}$, and the carrier concentration was $3 \times 10^{18}\,cm^{-3}$. Undoped GaN layers of 2 μm thickness were grown on the substrates for isolation between the p-type active layer and the n-type substrate. For the active layer, 1-μm thick low-Mg-doped GaN (Mg content of $1 \times 10^{18}\,cm^{-3}$) and low-Mg-doped (Mg content of $1 \times 10^{18}\,cm^{-3}$) (a) p-GaN, (b) p-$In_{0.02}Ga_{0.98}N$, or (c) p-$Al_{0.02}Ga_{0.98}N$ layers were grown on the undoped GaN. The Mg-doping concentration was confirmed to be 1×10^{18} cm^{-3} by secondary ion mass spectrometry (SIMS). The Al and In compositions were determined to be 2% by photoluminescence (PL) and X-ray diffraction measurements. We also prepared AlGaN samples with Al contents of (d) 4% and (e) 7% on sapphire substrates. After cleaning with an organic solvent and buffered-hydrofluoric-acid surface treatment, 50-nm thick Ni and 50-nm thick Au films were successively deposited by electron-beam evaporation to form Schottky contacts (Ø 200–500 μm), and large-area indium-gallium alloy ohmic electrodes were formed. After the device fabrication, I–V measurements were subsequently conducted for testing ohmic contacts. It was confirmed that the ohmic resistance was small enough for this study.

First, the I–V measurements were carried out to analyze the basic electronic characteristics by using an HP4142B semiconductor parameter analyzer. The $q\phi_B$ was calculated with respect to the thermionic emission model [12] using

$$J = A^{**}T^2\exp(-q\varphi_B/kT)[\exp(qV/kT) - 1], \tag{1}$$

where A^{**} is the effective Richardson constant (75 $A/cm^2\,K^2$ for p-GaN based on $A^{**} = 4\pi m^* qk^2/h^3$ and $m^* = 0.60m_0$), T is the temperature, q is the charge of the electron, k is the Boltzmann constant, and V is the applied voltage. The measurements were done in a same manner as in the previous report [9]. A sample with circular dots 200–500 μm in diameter was loaded in a measurement box, and then a pair of probes was attached to the ohmic and Schottky contacts. The sample was illuminated by white light. The light went through the gap region between the contacts, and was reflected back at the metallic sample-mounting base. By doing so, the light illuminated both the semiconductor layer and the metal/semiconductor interface. Subsequently, the viewing window was closed to darken the interior of the box, and the first voltage sweep from 0 to −10 V was done. Just after the first sweep, the second voltage sweep started successively.

PR measurements were also carried out. This method is known to be effective for samples with a large leakage current because the photocurrent can be detected without bias. When a monochromatic light with a photon energy ($h\upsilon$) greater than $q\phi_B$ is incident on the metal/GaN interface, electrons in the metal can surmount the Schottky barrier and a photocurrent is generated. Such a process is called the internal photoemission effect. The $q\phi_B$ is determined from photocurrent using Fowler's equation [13],

$$Y^{1/2} \propto (h\upsilon - q\varphi_B), \tag{2}$$

where Y is the photocurrent per photons. When $h\upsilon$ is close to the fundamental absorption edge, a large photocurrent flows because of the generation of electron–hole pairs as in a solar cell.

The H-ICTS was carried out to analyze the surface defects. Under a reverse bias voltage (V_{bias}), the depletion layer capacitance of a metal/p-GaN contact with acceptor-type ionized traps $N_T(t)$ is expressed as

$$C(t)^2 = \frac{q\epsilon A^2(N_A + N_T(t))}{2(V_{bi} - V_{bias})}, \tag{3}$$

where q is the electronic charge, ϵ is the dielectric constant, A is the junction area, N_A is the shallow acceptor concentration, and V_{bi} is the built-in potential. After application of a filling pulse, the time-dependent diode capacitance $C(t)$ was measured and the ICTS signal S was obtained by the following equation [14]

$$S(t) = t \times \frac{d\{C^2(t) - C^2(\infty)\}}{dt}. \tag{4}$$

The measurements were conducted at elevated temperatures of 130, 145, 160, and 175 °C to enhance the thermal

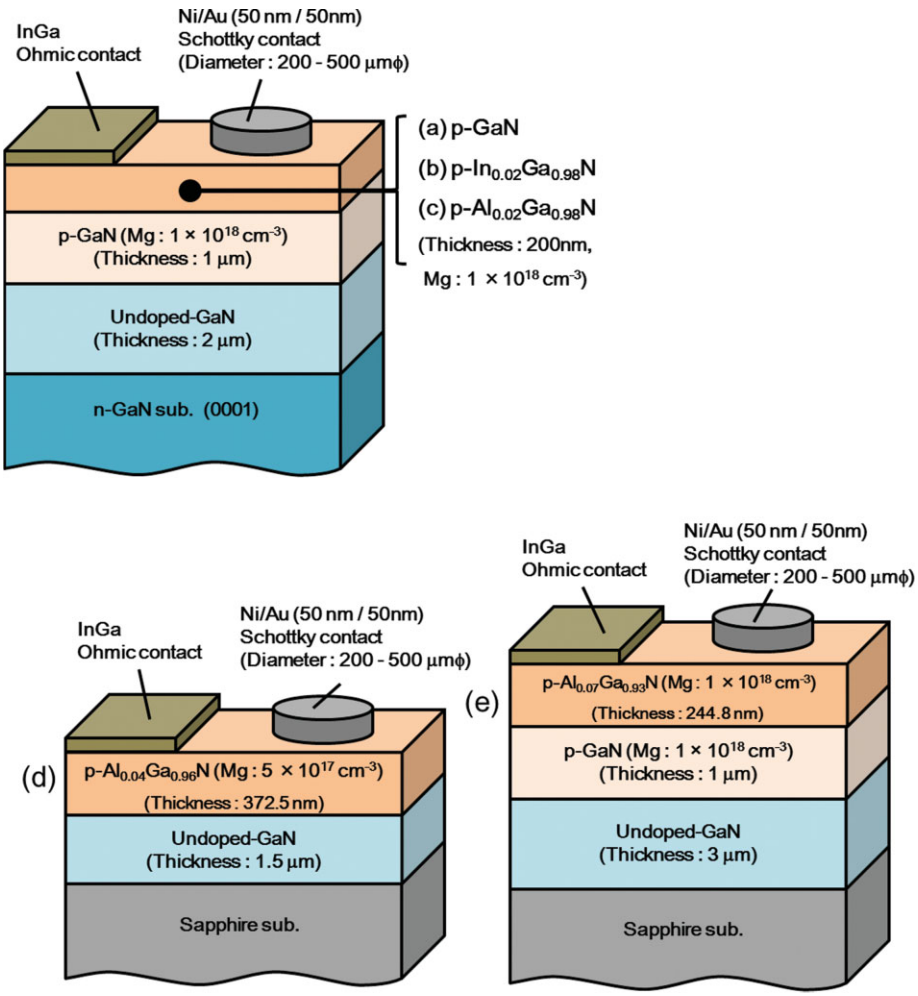

Figure 2 Schematic cross-sectional views of the metal/low-Mg-doped (a) p-GaN, (b) p-InGaN, and (c)–(e) p-AlGaN contacts.

emission from the defect levels, which in the present case are substantially deep. In the series of samples prepared, the ICTS signal was not detected when the filling and bias voltage conditions were specifically set for detecting defects near the depletion layer edge. In this study, since we focused on the defects in the vicinity of the interface we chose a forward filling pulse of 10 V for 1 min and a stationary bias of 0 V as in the previous study [15].

3 Experimental results

3.1 Forward *I–V* characteristics We show in Fig. 3 typical forward *I–V* curves of the Au/Ni/p-GaN, p-AlGaN, and p-InGaN samples in a semilog plot. After the white-light illumination, the forward voltage was swept twice from 0 to −10 V in the dark. For the p-type GaN sample, we observed in the first curve an exponential current increase in a voltage range between −0.1 and −0.8 V, representing a lower $q\phi_B$. This is followed by a small current decrease at a voltage beyond −0.8 V. In the voltage range $-10\,\text{V} < V < -5\,\text{V}$, the current monotonically increased. In the second curve, we observed a much smaller current than that in the first sweep

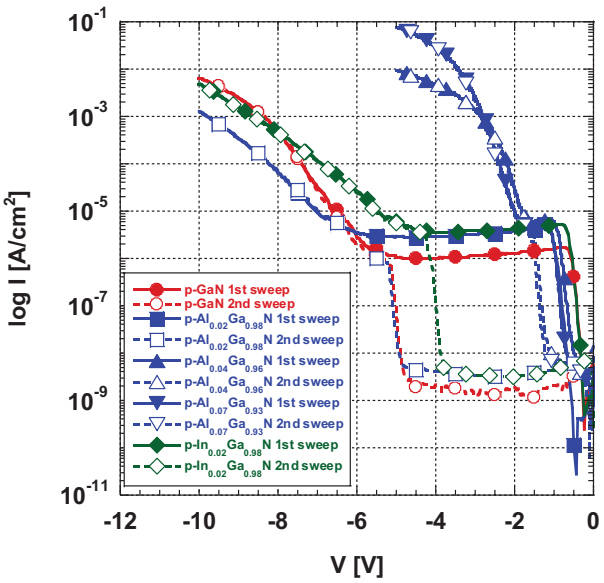

Figure 3 Typical forward *I–V* curves of Au/Ni/p-GaN, p-AlGaN, and p-InGaN samples in a semilogarithm plot.

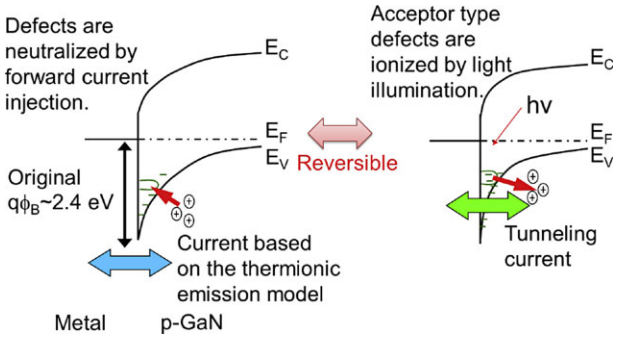

Figure 4 Band diagrams of a metal/low-Mg-doped p-GaN contact.

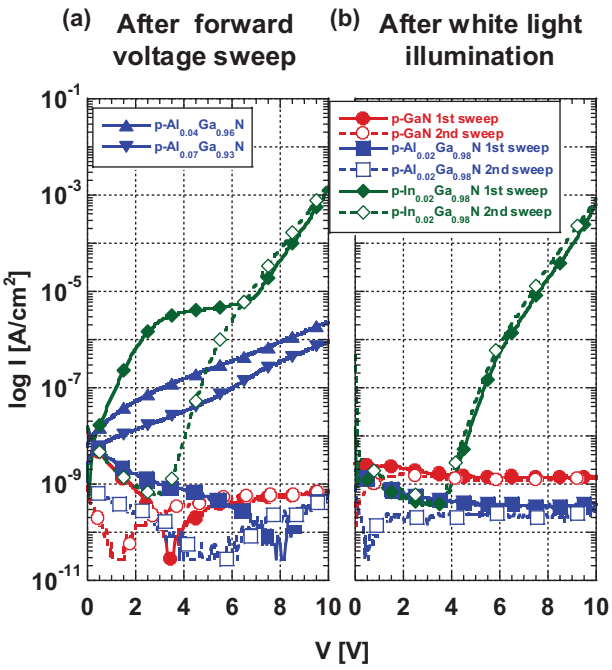

Figure 5 Typical reverse *I–V* curves of Au/Ni/p-GaN, p-AlGaN, and p-InGaN samples after (a) the forward-voltage sweep and (b) white-light illumination in semilogarithm plots.

in the voltage range between 0 and −4.5 V following by an exponential increase around −5 V, and a continuous increase as in the first sweep. The increase in the voltage around −5 V infers a higher $q\phi$. Such behaviors were repeatedly observed as we repeated the white-light irradiation and the forward-bias sweep: We call this phenomenon the memory effect. The memory effect is repeatable due to charge and discharge of holes to acceptor-type defects [10]. As mentioned in the introduction, the acceptor-type defects were fully ionized by the white-light irradiation before the measurements: We present a figure schematically showing such light-induced ionization in Fig. 4 on the right. As the interface acceptor defects exist in a high density, the depletion layer width became thin upon ionization. As a result, in the first sweep, the apparent $q\phi_B$ is low because the current can tunnel through the thin depletion layer. The defects were neutralized by the first voltage sweep, as shown on the left side of Fig. 4. In the second sweep, the depletion layer width returned to the initial width before white-light illumination. In such a circumstance, the thermionic emission current is dominating, and the intrinsic high $q\phi_B$ may be observed. Such a phenomenon is usually observed in the *I–V* and capacitance–voltage (*C–V*) characteristics of low-Mg-doped p-GaN contacts [9]. As shown in Fig. 1, the sample with a relatively high Al content in $Al_xGa_{1-x}N$ and also with a high Mg concentration was very leaky. By contrast, in the p-$Al_{0.02}Ga_{0.98}N$ and p-$In_{0.02}GaN$ samples as well as in the p-GaN samples, the *I–V* characteristics were significantly improved. It is noted that the memory effect was observed in the *I–V* characteristics. In the p-$In_{0.02}Ga_{0.98}N$ sample, the onset voltage where the current begins exponentially increasing shifts by about 1 V as compared to those of $Al_{0.02}Ga_{0.98}N$ and GaN in the second *I–V* curve. In the p-$Al_{0.04}Ga_{0.96}N$ and p-$Al_{0.07}Ga_{0.93}N$ samples, the onset voltages in the second curves were greatly shifted, thereby the memory effect was much less pronounced. Therefore, the second *I–V* curves give reduced $q\phi_B$.

3.2 Reverse *I–V* characteristics In order to clarify the effect of the charge state of the interfacial defects, we successively carried out the reverse *I–V* measurements twice, either after the neutralization of the defects by a forward current sweep or after the ionization by white-light illumination. We present the results in Fig. 5. In the p-$Al_{0.04}Ga_{0.96}N$ and p-$Al_{0.07}Ga_{0.93}N$ samples, the reverse current was 1–3 × 10^{-6} A/cm^2 at 10 V. In contrast, in the p-GaN and p-$Al_{0.02}Ga_{0.98}N$ samples, the reverse current was between 1 × 10^{-10} to 10 $^{-9}$ A/cm^2 after either the current injection or the illumination. In the p-$In_{0.02}Ga_{0.98}N$ samples, in the first reverse-bias sweep after the forward-bias sweep, the current steeply increases in voltage from 0 to 2.5 V, and plateaus around 6.5 V, and then increases again until the voltage reaches to 10 V, as shown in Fig. 5a. The current was 1.5 × 10^{-3} A/cm^2 at 10 V. In the second sweep, the current starts increasing at 4 V, and the first and second *I–V* curves overlap each other. After the illumination as shown in Fig. 5b, both the first and second *I–V* curves seem nearly identical to those taken by the second sweep after the forward-voltage sweep.

3.3 PR spectrum Figure 6 shows the PR spectrum for all the samples. The PR signals were not detected when $h\nu$ is below 2.0 eV. When $h\nu$ reaches 2.1–2.3 eV the signal starts to increase abruptly. The signals linearly increase until about 3.0 eV, thereby the $q\phi_B$ can be obtained by extrapolating the linearly increasing portion and reading the intersecting energy based on Eq. (2). When $h\nu > 3.0$ eV, the signals steeply increase, reflecting the onset of the fundamental absorption. At just below 3.5 eV, the signals dropped. This is because the back illuminated incident light was completely absorbed within the GaN free-standing

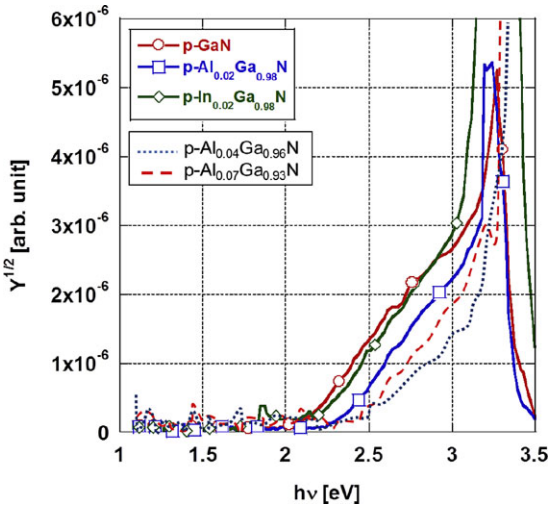

Figure 6 PR spectrum of the Au/Ni/p-GaN, p-AlGaN, and p-InGaN samples.

substrate and could not reach the metal/semiconductor interface.

3.4 Schottky barrier height Figure 7 shows $q\phi_B$ obtained from the *I–V* and PR results. The $q\phi_B$ obtained from the first voltage sweep in the *I–V* measurement was 1.10, 1.22, and 1.06 eV for p-GaN, p-$Al_{0.02}Ga_{0.98}N$, and p-$In_{0.02}Ga_{0.98}N$ samples, respectively. These $q\phi_B$ values are low, because the tunneling current is dominating as explained in Fig. 4. The second *I–V* sweep gave $q\phi_B$ values of 3.31, 3.04, and 2.99 eV, respectively, for p-GaN, p-$Al_{0.02}Ga_{0.98}N$, and p-$In_{0.02}Ga_{0.98}N$ samples. We find a large variation in $q\phi_B$ obtained from the *I–V* measurement probably due to the memory effect. For the p-$Al_{0.04}Ga_{0.96}N$ and p-$Al_{0.07}Ga_{0.93}N$ samples, the $q\phi_B$ values obtained from the first sweep are 1.15 and 1.04 eV, respectively. Those obtained from the second sweep are 1.48 and 1.58 eV respectively for p-$Al_{0.04}Ga_{0.96}N$ and p-$Al_{0.07}Ga_{0.93}N$ samples: they are much lower than those obtained in the sample with Al content of 2%. In contrast, the PR measurements can determine $q\phi_B$ without suffering from the memory effect: we obtained 2.09 eV for p-GaN samples, and values higher by 0.21, 0.25, 0.27 and 0.17 eV, respectively, for p-$Al_{0.02}Ga_{0.98}N$, p-$Al_{0.04}Ga_{0.96}N$, p-$Al_{0.07}Ga_{0.93}N$, and p-$In_{0.02}Ga_{0.98}N$ samples. We obtained for the p-$Al_{0.04}Ga_{0.96}N$ and p-$Al_{0.07}Ga_{0.93}N$ samples 2.34 and 2.36 eV, respectively, where we have high $q\phi_B$ values even when the samples were leaky as compared to those obtained from the *I–V* measurement.

3.5 High-temperature ICTS spectra and Arrhenius plots Figure 8 shows the H-ICTS spectra for the p-GaN, p-$Al_{0.02}Ga_{0.98}N$ and p-$In_{0.02}Ga_{0.98}N$ samples measured at 175 °C. We observe in all spectra a large single peak within a one and a half digit time domain. The peak positions were 327, 518, and 284 s for p-GaN, p-$Al_{0.02}Ga_{0.98}N$, and p-$In_{0.02}Ga_{0.98}N$, respectively. Figure 9 shows Arrhenius plots obtained for temperatures of 130, 145, 160, and 175 °C. Table 1 summarizes the defect parameters of trap energy (E_t), capture cross section, and interfacial states density. The trap energies were $E_V + 0.906$, $E_V + 0.915$, and $E_V + 0.839$ eV for p-GaN, p-$Al_{0.02}Ga_{0.98}N$, and p-$In_{0.02}Ga_{0.98}N$, respectively. We have conducted H-ICTS measurements with various combinations of filling pulse and bias voltages [15]. Under conventional measurement conditions, we measure a contribution of defects distributed within most of the

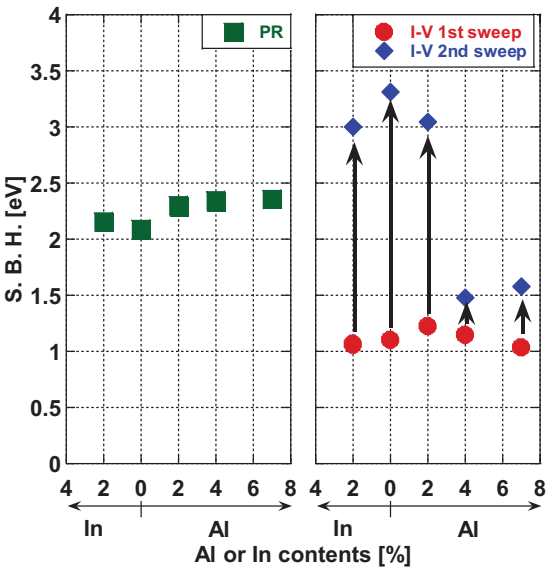

Figure 7 Schottky-barrier height measured from the *I–V* and PR results.

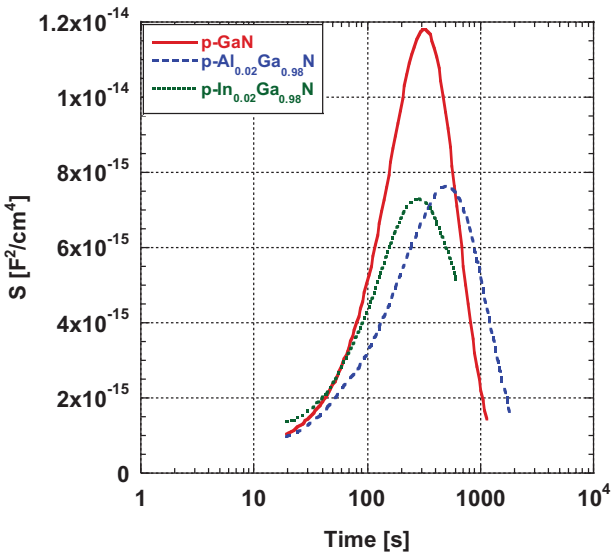

Figure 8 High-temperature ICTS spectra measured for the p-GaN, p-$Al_{0.02}Ga_{0.98}N$, and p-$In_{0.02}Ga_{0.98}N$ samples.

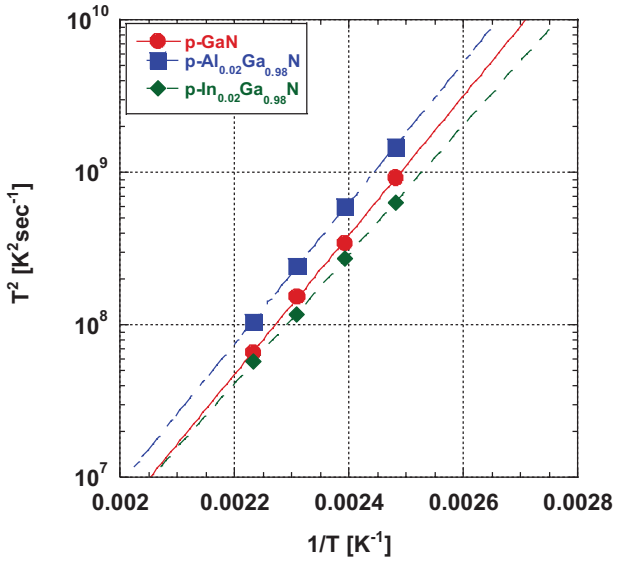

Figure 9 Arrhenius plots for the ICTS peaks.

Table 1 Defect parameters, trap energy, capture cross–section, and interfacial states densities, obtained from the Arrhenius plot.

	p-GaN	p-AlGaN	p-InGaN
E_t [eV]	$E_V + 0.906$	$E_V + 0.915$	$E_V + 0.839$
σ_p [cm^2]	9.51×10^{-19}	7.50×10^{-19}	1.97×10^{-19}
N_t [cm^{-2}]	1.41×10^{13}	8.23×10^{12}	7.38×10^{12}

depletion layer, including the edge region. Virtually, we detected no ICTS signal near the depletion layer edge. However, when we applied a large forward filling voltage accompanied by a large current, a large single peak was observed, as in Fig. 8. Therefore, the defects were located in the vicinity of the interface. Because we did not know depth profile of the defects, we expressed the number of defects in density per unit cm^2 (N_t). We estimated the N_t values as 1.41×10^{13}, 8.23×10^{12}, and 7.38×10^{12} cm^{-2} for p-GaN, p-$Al_{0.02}Ga_{0.98}N$, and p-$In_{0.02}Ga_{0.98}N$, respectively. We note that N_t values in the $Al_{0.02}Ga_{0.98}N$ and $In_{0.02}Ga_{0.98}N$ samples are about half that in the GaN sample.

4 Discussion We have observed the memory effect in the $Al_{0.02}Ga_{0.98}N$ and $In_{0.02}Ga_{0.98}N$ samples and a large single H-ICTS peak. We have reported in our previous papers [15, 16] that the origin of this peak in the p-GaN samples is the gallium vacancy (V_{Ga}) near to the interface. On the other hand, it has been reported that the Al vacancy (V_{Al}) and/or the In vacancy (V_{In}) also exist in AlGaN and/or InGaN with high Al and/or In contents [17, 18]. However, in this study, because the Al and In contents are only 2% and a similar E_t is observed across the samples, we speculated that the dominant contribution of the main peak is V_{Ga}. We considered that as long as c-plane crystals are used, V_{Ga} is formed at the p-$Al_{0.02}Ga_{0.98}N$ and p-$In_{0.02}Ga_{0.98}N$ surfaces. Because these samples were grown by MOCVD, we speculate surface structures including Ga atoms on top shown in Fig. 10a: while the surface was terminated by hydrogen, oxygen, or carbon atoms [19, 20], we expect that V_{Ga} values may be easily formed. However, the memory effect is less pronounced in the p-$In_{0.02}Ga_{0.98}N$ sample and N_t decreases in the $Al_{0.02}Ga_{0.98}N$ and $In_{0.02}Ga_{0.98}N$ samples. These results suggest that in the p-$Al_{0.02}Ga_{0.98}N$ and p-$In_{0.02}Ga_{0.98}N$ samples the surface morphology became poor, and a larger fraction of Ga atoms at the surface were missing, as shown in Fig. 10b. We thus consider that the formation of V_{Ga} is partly hindered. On the other hand, for the $Al_{0.04}Ga_{0.96}N$ and $Al_{0.07}Ga_{0.93}N$ samples, the I–V characteristics were leaky. It is thus suggested that the crystal quality already deteriorated even though the Al content was only 4%.

In the p-$In_{0.02}Ga_{0.98}N$ sample, the large leakage current was observed, especially in the first sweep after the application of forward bias. It is speculated that relatively shallow acceptor-type interfacial defects were formed, and a current can flow via the defects. The current, originating from the hole emission from the defects, was observed in the first sweep. As the indium atom has large atomic radius, the wavefunction spreads in a large extent. Therefore, even though the In concentration is only 2%, a surface defect continuum might exist close to the valence band. For the future study, we will conduct ICTS measurements in a shorter time range to analyze shallower surface defect continuum.

The energy gap (E_g) of the p-AlGaN (p-InGaN) samples can be calculated by using Vegard's law in the following equation:

$$E_{g(Al(In)_xGa_{1-x}N)} = (1-x)E_{g(GaN)} + xE_{g(Al(In)N)} - bx(1-x), \quad (5)$$

where $E_{g(GaN)}$ and $E_{g(AlN)}$ [$E_{g(InN)}$] are the E_g values of GaN and AlN (InN), respectively, x is the atomic fraction of Al

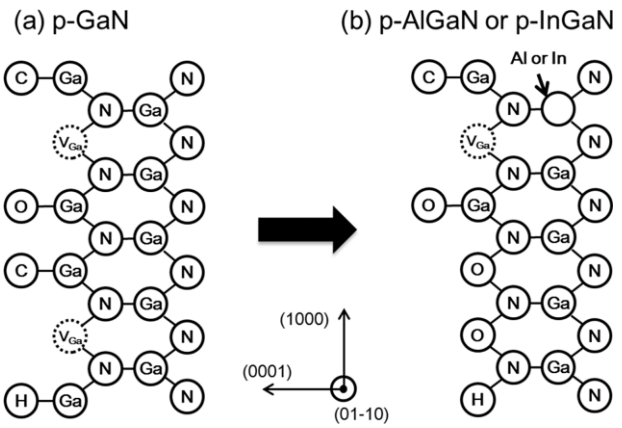

Figure 10 Models for surface crystal structures of c-plane (a) GaN and (b) AlGaN or InGaN.

(In), b is the bowing parameter. We used $E_{g(GaN)} = 3.39$, $E_{g(AlN)} = 6.20$, $E_{g(InN)} = 0.70$, and $b = 1.00$ eV.

The calculated E_g varied according to the increase of the composition by 37 meV for $Al_{0.02}Ga_{0.98}N$, 74 meV for $Al_{0.04}Ga_{0.96}N$, 137 meV for $Al_{0.07}Ga_{0.93}N$,and decreases by −73 meV for $In_{0.02}Ga_{0.98}N$. Supposing that half of the E_g change turns in a $q\phi_B$ change, the $q\phi_B$ varied by +18.5, +37.0, +68.5, and −36.5 meV for $Al_{0.02}Ga_{0.98}N$, $Al_{0.04}Ga_{0.96}N$, $Al_{0.07}Ga_{0.93}N$, and $In_{0.02}Ga_{0.98}N$ samples, respectively. However, the $q\phi_B$ value changes from the PR measurement are +0.21, +0.25, +0.27, and +0.17 eV for $Al_{0.02}Ga_{0.98}N$, $Al_{0.04}Ga_{0.96}N$, $Al_{0.07}Ga_{0.93}N$, and $In_{0.02}Ga_{0.98}N$ samples, respectively. A possible explanation for these discrepancies may be from the net charge of the interfacial states. The acceptor-type defect densities of $Al_{0.02}Ga_{0.98}N$ and $In_{0.02}Ga_{0.98}N$ surfaces are half that in the GaN. The electric field at the interface was relaxed, and the barrier lowering decreased, which enhances the $q\phi_B$. As a counter effect, for the $In_{0.02}Ga_{0.98}N$ samples, shallow acceptor-type defects might be formed, which decreases $q\phi_B$. Finally, the measured $q\phi_B$ values in the $In_{0.02}Ga_{0.98}N$ samples were smaller than that in the $Al_{0.02}Ga_{0.98}N$ samples.

5 Conclusions The electrical characteristics of low-Mg-doped p-$Al_{0.02}Ga_{0.98}N$, p-$Al_{0.04}Ga_{0.96}N$, p-$Al_{0.07}Ga_{0.93}N$, and p-$In_{0.02}Ga_{0.98}N$ Schottky contacts were investigated. In the I–V results, we observed memory effects. It was found that the interfacial defect density in the $Al_{0.02}Ga_{0.98}N$ and $In_{0.02}Ga_{0.98}N$ samples were almost half that observed in the GaN samples. It was considered that V_{Ga} in the vicinity of the interface decreased due to the poor surface morphology of $Al_{0.02}Ga_{0.98}N$ and $In_{0.02}Ga_{0.98}N$. A large leakage current was observed in the $In_{0.02}Ga_{0.98}N$ contacts. This may be accounted for by assuming relatively shallow acceptor-type interfacial defects formed and a current flow via the defects. We also observed current contribution originating from the hole emission from the defects. In the p-$Al_{0.04}Ga_{0.96}N$ and p-$Al_{0.07}Ga_{0.93}N$ samples, the I–V characteristics were leaky. The $q\phi_B$ estimated from the PR experiment were higher than the values estimated from the bandgap by 0.19, 0.21, 0.20, and 0.21 eV for $Al_{0.02}Ga_{0.98}N$, $Al_{0.04}Ga_{0.96}N$, $Al_{0.07}Ga_{0.93}N$, and $In_{0.02}Ga_{0.98}N$ samples, respectively. A probable explanation for such discrepancies may be due to the total charge amount of the interfacial states, which varied the electric field and the barrier lowering. It was found that even though the Al or In content was only as small as 2%, the electrical characteristics of the contacts changed significantly.

Acknowledgements A part of this work was supported by a Grant-in-Aid for Scientific Research C from the Ministry of Education, Culture, Sports, Science, and Technology.

References

[1] S. Nakamura, M. Senoh, S. Nagahama, N. Iwasa, T. Yamada, T. Matsushita, H. Kiyoku, and Y. Sugimoto, Jpn. J. Appl. Phys. **35**, L74 (1996).
[2] L. Zhou, A. T. Ping, F. Khan, A. Osinsky, and I. Adesida, Electron. Lett. **36**, 91 (2000).
[3] J.-S. Jang, S. J. Park, and T.-Y. Seong, J. Vac. Sci. Technol. B **17**, 2667 (1999).
[4] Y. Koide, T. Maeda, T. Kawakami, S. Fujita, T. Uemura, N. Shibata, and M. Murakami, J. Electron. Mater. **28**, 341 (1999).
[5] J.-S. Jang, S. J. Park, and T.-Y. Seong, Appl. Phys. Lett. **76**, 2898 (2000).
[6] L. S. Yu, D. J. Qiao, Q. J. Xing, S. S. Lau, K. S. Boutros, and J. M. Redwing, Appl. Phys. Lett. **73**, 238 (1998).
[7] K. Mochizuki, A. Terano, N. Kaneda, T. Mishima, T. Ishigaki, and T. Tsuchiya, Appl. Phys. Express **4**, 024104 (2011).
[8] R. Padma, B. P. Lakshmi, M. S. P. Reddy, and V. R. Reddy, Superlattices Microstruct. **56**, 64 (2013).
[9] K. Shiojima, T. Sugahara, and S. Sakai, Appl. Phys. Lett. **74**, 1936 (1999).
[10] K. Shiojima, T. Sugahara, and S. Sakai, Appl. Phys. Lett. **77**, 4353 (2000).
[11] K. Shiojima, T. Takahashi, N. Kaneda, T. Mishima, and K. Nomoto, Jpn. J. Appl. Phys. **52**, 08JJ08 (2012).
[12] S. M. Sze, Physics of Semiconductor Devices, 2nd edn. (Wiley, New York, 1981), pp. 245–311.
[13] R. H. Fowler, Phys. Rev. **38**, 45 (1931).
[14] H. Okushi and Y. Tokumaru, Jpn. J. Appl. Phys. **20**, 261 (1981).
[15] K. Shiojima, S. Sugitani, and S. Sakai, Appl. Surf. Sci. **190**, 318 (2002).
[16] K. Shiojima, H. Wakayama, T. Aoki, N. Kaneda, K. Nomoto, and T. Mishima, Thin Solid Films **557**, 268 (2014).
[17] A. Uedono, K. Tenjinbayashi, T. Tsutsui, Y. Shimahara, H. Miyake, K. Hiramatsu, N. Oshima, R. Suzuki, and S. Ishibashi, J. Appl. Phys. **111**, 013512 (2012).
[18] A. Uedono, S. Ishibashi, N. Oshima, R. Suzuki, and M. Sumiya, ECS Trans. **61**, 19 (2014).
[19] V. M. Bermudez, Surf. Sci. **565**, 89 (2004).
[20] V. M. Bermudez, J. Appl. Phys. **80**, 1190 (1996).